JOURNAL OF CHEMICAL PHYSICS VOLUME 120, NUMBER 19 15 MAY 2004

Kinematic effects associated with molecular frames in structural isomerization dynamics of clusters

Tomohiro Yanao[a] and Kazuo Takatsuka[b]
Department of Basic Science, Graduate School of Arts and Sciences, University of Tokyo, Komaba, 153-8902, Tokyo, Japan

(Received 17 November 2003; accepted 18 February 2004)

Kinematic effects associated with movements of molecular frames, which specify instantaneous orientation of molecules, is investigated in structural isomerization dynamics of a triatomic cluster whose total angular momentum is zero. The principal-axis frame is employed to introduce the so-called principal-axis hyperspherical coordinates, with which the mechanism of structural isomerization dynamics of the cluster is systematically analyzed. A force called ''democratic centrifugal force'' is extracted from the associated kinematics. This force arises from an intrinsic non-Euclidean metric in the internal space and has an effect of distorting the triatomic cluster to a collapsed shape and of trapping the system around collinear transition states. The latter effect is particularly important in that the kinematics effectively makes a basin at the saddle (transition state) on the potential surface. Based on this framework, we study the effect of the gauge field associated with the Eckart frame in internal space, which has not been carefully examined in the conventional reaction rate theories. Numerical comparison between the dynamics with and without the gauge field has revealed that this field has an effect to suppress the rate of isomerization reaction to a considerable amount. Thus a theory neglecting this effect will significantly overestimate the rate of isomerization. We show the physical origin of this suppressing effect. [DOI: 10.1063/1.1698616]

I. INTRODUCTION

Structural isomerization dynamics of small clusters provides many a novel feature in chemical dynamics that are still to be explored. They are characterized as a typical large-amplitude collective motion, which also constitutes important processes in wide varieties of polyatomic molecules, such as conformational change of polymers, crystals, glassy systems, and so on. Therefore the cluster dynamics have been approached from various viewpoints: microcanonical analog of solid-liquid phase transitions[1,2] and a prototype of multichannel chemical reactions.[3] They are sometimes studied with an emphasis on chaos and regularity in Hamiltonian many-body systems.[4–6] Since potential-energy topography is considered to dominate reaction dynamics in the standard chemical reaction theories,[7,8] the potential landscape for cluster dynamics[9,10] and the free-energy landscape for protein folding[11,12] have been explored very extensively. However, it is too naive to attribute all the dynamics to the potential topography alone. This is because a very significant, both qualitatively and quantitatively, force can arise from the kinematics too, which can compete with the force due to the potential. Exploring and identifying such a force and its effects are among the major concerns in this paper.

In expressing the kinetic energy of an n-atom $(n \geqslant 3)$ system in terms of $3n-6$ internal variables, one faces the problem of separation of rotations and internal motions. This problem remains even in a system of vanishing total angular momentum. It is often illustrated in terms of the ''falling cat'' effect[13] that an isolated deformable body with zero angular momentum can change its orientation with a change of its shape. This remarkable effect is quite universal in nature from fundamental three-body systems[14] to various living bodies.[15] Nonseparability between vibrational and rotational motions is also essential in the isomerization dynamics of clusters: A cluster with zero angular momentum actually changes its orientation gradually with the small vibration, and this effect is even more vital in the large amplitude structural isomerization. Strictly speaking, however, the orientation of a molecule can be uniquely identified only after a definite decision of molecular shape is made. Therefore it is a usual practice to define an instantaneous molecular orientation in terms of a continuous change of molecular (body) frame. The falling cat effect simply implies that a rotation-free body frame does not exist in general. Nevertheless, referring to such a moving body frame, a $(3n-6)$-dimensional internal dynamics for molecular shape can be extracted.

The problem of separation of internal and rotational motions dates back to the 1930s due to the monumental work by Eckart.[16] He exploited the so-called ''Eckart frame'' for an approximate separation of rotational and vibrational modes for semirigid molecules around their local equilibrium structures.[17–19] The Eckart frame is widely used for the normal-mode analysis in the vicinity of local equilibrium structure since it (approximately) factors out a $(3n-6)$-dimensional Euclidean subspace. The Eckart idea of constructing the internal subspace has been further developed in the theory of ''reaction path Hamiltonian'' due to

---

[a] Electronic address: yanao@mns2.c.u-tokyo.ac.jp
[b] Electronic address: kaztak@mns2.c.u-tokyo.ac.jp

Miller *et al.*,[20] where the Eckart condition is assigned along a reaction path. Hinde and Berry[5] also employed a procedure similar to the Eckart condition[21] for the instantaneous normal-mode analysis to eliminate the infinitesimal rotational degrees of freedom in the Morse and Lennard-Jones clusters.

However, it should be recalled that the separation of internal motions and rotational motions is not globally accomplished by invoking the Eckart procedure. Thus more elaborated gauge-theoretical approaches have been developed by Guichardet,[22] Tachibana and Iwai,[23,24] and Littlejohn and Reinsch.[25] These theories tell that a gauge field inevitably arises in internal space when a body frame is introduced. Furthermore, the gauge field thus born couples with the Euclidean metric of configuration space resulting in a non-Euclidean metric in the internal space. This means that dynamics in thus determined internal space is inevitably influenced by ‘‘metric force,’’ which is different from the usual potential force. An important relevant fact is that the effect of such a metric force is never small as quantified in this paper.

The aim of this paper studying the isomerization reaction in a triatomic cluster is twofold. First, by employing a coordinate system called the principal-axis hyperspherical coordinates (PAHC’s) developed earlier by Zickendraht[26] and later by Chapuisat *et al.*[27–29] and Kuppermann,[30] where the internal motion of a molecule is described in terms of gyration radii and hyperangles referring to the principal axes of moment of inertia tensor of the molecule at each instant, we identify the kinematic force explicitly that is called ‘‘democratic centrifugal force (DCF)’’ on the space of the gyration radii. This force is generated by the change of the hyperangle called kinematic or democratic rotation.[25,31–35] We show that this coordinate system is particularly suitable to describe the collective motion of isomerization dynamics, since only a couple of independent variables play a predominant role as a collective coordinate. We clarify the kinematic effects of the DCF both theoretically and numerically. In particular, we find that DCF drives a triatomic cluster to change its shape from equilateral to collinear configurations, thus helping isomerization to begin. In addition, the DCF works to trap a molecule in the region of the collinear transition state. By constructing an effective potential, we give a geometrical view of the origin of such a trapping motion, thereby accounting for the recrossing problem in chemical reaction dynamics in a unified manner.

The second aim of the present paper is to elucidate the effects of the gauge field in the internal space associated with the Eckart frame in application to the isomerization reaction of cluster. The motivation of this study lies in the fact that the gauge field arising from the Eckart frame is often disregarded in many studies of molecular vibrations and that most attention tend to be concentrated on the effects of potential-energy topography. For small-amplitude vibrations around a reference molecular configuration, the gauge-field effect may be negligible since the Eckart frame makes the gauge field vanish at the reference configuration. However, this is not necessarily the case with large-amplitude motions like isomerizations and chemical reactions. In order to quantify a possible error in such theoretical treatments that neglect the gauge field, we compare two dynamics: one is a full dynamics under a correct gauge field and the other is a dynamics in which the gauge field is totally eliminated. It turns out that the gauge field generally tends to suppress the rate of isomerization reaction significantly. A theoretical mechanism of this suppressing effect is discussed in terms of the PAHC’s.

The present paper is organized as follows. In Sec. II, after introducing our model clusters, we briefly summarize the gauge-theoretical treatment of internal motions of general *n*-atom systems following a similar manner as Littlejohn and Reinsch.[25] In Sec. III, the mechanism of the isomerization reaction is elucidated in terms of the principal-axis hyperspherical coordinates (PAHC’s). Roles of the democratic centrifugal force are highlighted. In Sec. IV, we investigate the significant effect of the gauge field associated with the Eckart frame on the rate of the structural isomerization of a triatomic cluster. This paper concludes in Sec. V with some remarks.

II. A BRIEF SUMMARY OF A GAUGE-THEORETICAL FORMALISM FOR INTERNAL MOTIONS IN PRINCIPAL-AXIS HYPERSPHERICAL COORDINATES FOR ISOMERIZATION DYNAMICS

A. Model cluster: M_3

We study a cluster composed of three identical atoms that interact through the pairwise Morse potential M_3. Total angular momentum of the system is zero throughout. The Hamiltonian $\mathcal{H}/\varepsilon$ of this system has the following dimensionless form:

$$\frac{\mathcal{H}}{\varepsilon}=\frac{1}{2}\sum_{i=1}^{3}(\dot{\mathbf{r}}_{si}\cdot\dot{\mathbf{r}}_{si})+\sum_{i<j}[e^{-2(d_{ij}-d_0)}-2e^{-(d_{ij}-d_0)}], \quad (1)$$

where a three-dimensional vector $\mathbf{r}_{si}=(r_{six},r_{siy},r_{siz})^T$ represents the position of the *i*th particle with respect to a space-fixed frame. The subscript s on $\mathbf{r}_{si}$ represents a quantity referred to a space-fixed frame. As will be introduced later, a vector $\boldsymbol{\rho}_i$ without subscript s represents a position vector relative to a body frame. This convention is adopted for other quantities throughout. ε represents the depth of the Morse potential and d_{ij} is the interparticle distance between the *i*th and *j*th atoms. The parameter d_0, which corresponds to the equilibrium distance of the pairwise Morse potential, controls the Hamiltonian and we set this parameter to $d_0=6.0$, which provides a potential topography similar to that of the Lennard-Jones potential that is frequently used to model the van der Waals clusters. The masses of all particles can be set to unity. In what follows, our numerical results are presented in the absolute units.

The M_3 cluster has two local equilibrium structures on its potential-energy surface corresponding to the two permutationally distinct equilateral triangle structures whose potential energy is $V=-3.00\varepsilon$, whereas it bears three permutationally distinct collinear saddle structures constituting a barrier height $V=-2.005\varepsilon$. These are summarized in Fig. 1. The system is laid on the $x-y$ plane with $r_{s1z}=r_{s2z}=r_{s3z}=0$ without loss of generality. Note that the two equilibrium

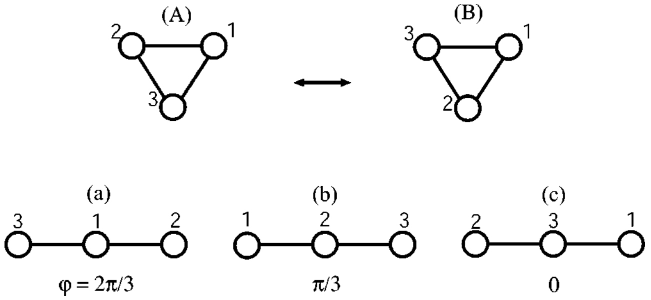

FIG. 1. Local equilibrium and saddle structures of triatomic Morse cluster M_3. This cluster has two permutationally distinct local equilibrium structures ($V=-3.00\varepsilon$) and three saddle structures ($V=-2.005\varepsilon$). The equilibrium structure is equilateral triangle and the saddle structure is collinear. Values for the hyperangle φ that specify respective saddle structures are denoted.

structures (A) and (B) in Fig. 1 are mutually distinctive, since the molecular motion is confined to its plane under zero total angular momentum.

B. Internal motions under zero angular momentum

To eliminate the translational degrees of freedom we begin with the mass-weighted Jacobi vectors. We next reduce the rotational degrees of freedom for the system of vanishing total angular momentum based on a gauge theoretical treatment.[25] For a rather general argument, we consider an n-atom molecule with $(n-1)$-Jacobi vectors $\{\boldsymbol{\rho}_{s1},\ldots,\boldsymbol{\rho}_{sn-1}\}$ in this subsection. Let a body frame (molecular frame) be represented by a 3×3 proper rotation matrix $R\in \mathrm{SO}(3)$, whose three column vectors represent the three orthonormal axes of the frame. R can be parametrized by the Euler angles $\{\theta^{\xi}\}$ ($\xi=1,2,3$) and thereby specifies the orientation of the axes. The body frame R is assigned for each configuration in a continuous manner and a rule of this assignment corresponds to a choice of a gauge convention in the gauge theory.[25] Among infinitely many possible choices of the body frame, we study the so-called principal-axis frame and the Eckart frame in this paper.

We briefly summarize some basic prerequisite facts that are common to any choice of the body frame. The mass-weighted Jacobi vectors referred to a body frame R, $\{\boldsymbol{\rho}_i\}$, are related to $\{\boldsymbol{\rho}_{si}\}$ as

$$\boldsymbol{\rho}_{si}=R(\{\theta^{\xi}\})\boldsymbol{\rho}_i(\{q^{\mu}\}) \quad (i=1,\ldots,n-1), \tag{2}$$

where $\{q^{\mu}\}\,(\mu=1,\ldots,3n-6)$ are internal coordinates that specify the molecular shape and are invariant under spatial rotation of the system. The angular momentum of the system about the center of mass, $\mathbf{L}_s=\Sigma_{i=1}^{n-1}\boldsymbol{\rho}_{si}\times\dot{\boldsymbol{\rho}}_{si}$, and that referred to the body frame $\mathbf{L}$ are also related mutually by the relation $\mathbf{L}_s=R\mathbf{L}$. Then $\mathbf{L}$ can be expressed by use of Eq. (2) and its time derivative as

$$\mathbf{L}=\sum_{i=1}^{n-1}\boldsymbol{\rho}_i\times(\boldsymbol{\omega}\times\boldsymbol{\rho}_i)+\sum_{i=1}^{n-1}\boldsymbol{\rho}_i\times\frac{\partial\boldsymbol{\rho}_i}{\partial q^{\mu}}\dot{q}^{\mu}, \tag{3}$$

where the sum convention is adopted for the index μ from 1 to $3n-6$. Likewise, we always adopt this convention for the indices μ and ν. The three-dimensional vector $\boldsymbol{\omega}$ is the angular velocity of the body frame (referred to the frame itself), whose relationship to the angular velocity matrix $\Omega\equiv R^T\dot{R}$ is expressed as

$$\Omega\equiv\begin{pmatrix} 0 & -\omega_3 & \omega_2 \\ \omega_3 & 0 & -\omega_1 \\ -\omega_2 & \omega_1 & 0 \end{pmatrix}\Leftrightarrow\boldsymbol{\omega}\equiv\begin{pmatrix}\omega_1\\ \omega_2\\ \omega_3\end{pmatrix}. \tag{4}$$

Equation (3) can be rewritten in a more compact form as

$$\mathbf{L}=M(\boldsymbol{\omega}+\mathbf{A}_{\mu}\dot{q}^{\mu}), \tag{5}$$

with M being the moment of inertia tensor referred to the body frame

$$M_{\alpha\beta}=\sum_{i=1}^{n-1}[(\boldsymbol{\rho}_i\cdot\boldsymbol{\rho}_i)\delta_{\alpha\beta}-\rho_{i\alpha}\rho_{i\beta}], \tag{6}$$

where $\delta_{\alpha\beta}$ is the Kronecker delta and the indices α and β specify axes of the body frame. $\mathbf{A}_{\mu}$ is a gauge potential defined by

$$\mathbf{A}_{\mu}=M^{-1}\left(\sum_{i=1}^{n-1}\boldsymbol{\rho}_i\times\frac{\partial\boldsymbol{\rho}_i}{\partial q^{\mu}}\right). \tag{7}$$

The kinetic energy K in the Jacobi vectors can also be expressed in terms of the quantities referred to the body frame using the time derivative of Eq. (2) as

$$K=\frac{1}{2}(\boldsymbol{\omega}^TM\boldsymbol{\omega})+(\boldsymbol{\omega}^TM\mathbf{A}_{\mu})\dot{q}^{\mu}+\frac{1}{2}h_{\mu\nu}\dot{q}^{\mu}\dot{q}^{\nu}, \tag{8}$$

where $h_{\mu\nu}$ is defined as

$$h_{\mu\nu}\equiv\sum_{i=1}^{n-1}\frac{\partial\boldsymbol{\rho}_i}{\partial q^{\mu}}\cdot\frac{\partial\boldsymbol{\rho}_i}{\partial q^{\nu}}. \tag{9}$$

The above expressions for the angular momentum [Eq. (5)] and the kinetic energy [Eq. (8)] are familiar in the conventional theory of molecular vibration.[16,17] The first, second, and third terms in the right-hand side of Eq. (8) are usually referred to as rotational kinetic energy, the Coriolis coupling term, and vibrational kinetic energy, respectively, and $h_{\mu\nu}$ looks like a metric tensor for molecular vibration. However, it should be noted that the decomposition in Eq. (8) depends on the choice of body frame, that is, gauge dependent. For example, the so-called Eckart frame[16–19] is a frame that makes the gauge potential $\mathbf{A}_{\mu}$ disappear at a local equilibrium configuration and makes the Coriolis coupling term negligible for small-amplitude vibration around the equilibrium. This Eckart procedure of the approximate separation of rotation and internal motion is convenient for the normal-mode analysis since the metric $h_{\mu\nu}$ happens to be Euclidean for the normal-mode coordinates $\{q^{\mu}\}$. However, it is crucial to note that $h_{\mu\nu}$ is not appropriate for the rigorous description of molecular internal motions including large-amplitude collective motions due to its dependence on the choice of body frame. For this reason $h_{\mu\nu}$ is called a pseudometric.[25] Significance of the distinction between the pseudometric $h_{\mu\nu}$ and the true metric introduced below is scrutinized in Sec. IV.

In Ref. 25, Littlejohn and Reinsch have shown a way of rearranging the kinetic energy of Eq. (8) into a gauge-invariant form based on the fiber-bundle picture of configuration space. The result is

$$K=\frac{1}{2}(\boldsymbol{\omega}+\mathbf{A}_\mu\dot{q}^\mu)^T M(\boldsymbol{\omega}+\mathbf{A}_\nu\dot{q}^\nu)+\frac{1}{2}g_{\mu\nu}\dot{q}^\mu\dot{q}^\nu, \tag{10}$$

where $g_{\mu\nu}$ is defined by

$$g_{\mu\nu}=h_{\mu\nu}-\mathbf{A}_\mu^T M\mathbf{A}_\nu. \tag{11}$$

Both of the first and the second terms on the right-hand side of Eq. (10) are gauge invariant. The former vanishes if and only if the total angular momentum $\mathbf{L}$ is zero [cf. Eq. (5)]. The metric tensor $g_{\mu\nu}$ in Eq. (11) is also gauge invariant and is the true metric appropriate for the description of internal motions in polyatomic molecules.

Thus the Lagrangian for an *n*-atom system of vanishing total angular momentum is reduced to

$$\mathcal{L}=\frac{1}{2}g_{\mu\nu}\dot{q}^\mu\dot{q}^\nu-V(\{q^\mu\}), \tag{12}$$

where we restrict ourselves to a system whose potential term depends only on the internal variables $\{q^\mu\}$ as in our M_3 cluster. Classical equations of motion for the internal coordinates $\{q^\mu\}$ are obtained straightforwardly by applying the Lagrangian Eq. (12) to the Euler–Lagrange equations as will be done in the following sections. Thus the internal motions of an *n*-atom system of vanishing total angular momentum are described in terms only of the $3n-6$ internal variables $\{q^\mu\}$. For more general expression for the equations of motion for a system of nonzero angular momentum, see Ref. 25.

A remarkable fact concerning the true metric $g_{\mu\nu}$ is that it is essentially non-Euclidean for three- or more-atom systems.[25] This implies that "metric forces" should arise from the internal dynamics that can compete with the usual force due to the potential energy. The kinematic effects owing to the metric force are our main concern in the following.

C. The principal-axis hyperspherical coordinates

We now introduce the so-called principal-axis hyperspherical coordinates (PAHC's) for the study of the structural isomerization dynamics of M_3 cluster. We start with a 3×2 matrix W_s composed of two Jacobi (column) vectors as

$$W_s\equiv(\boldsymbol{\rho}_{s1}\quad\boldsymbol{\rho}_{s2}), \tag{13}$$

where

$$\begin{aligned}\boldsymbol{\rho}_{s1}&=\sqrt{\mu_1}(\mathbf{r}_{s1}-\mathbf{r}_{s2}),\quad \mu_1=\frac{1}{2},\\ \boldsymbol{\rho}_{s2}&=\sqrt{\mu_2}\left(\frac{\mathbf{r}_{s1}+\mathbf{r}_{s2}}{2}-\mathbf{r}_{s3}\right),\quad \mu_2=\frac{2}{3}\end{aligned} \tag{14}$$

with μ_1 and μ_2 the reduced masses.[25,35] According to the singular value decomposition theorem,[36] W_s can be decomposed into a product of three matrices as

$$W_s=RNU^T \tag{15}$$

$$=(\mathbf{e}_1\quad\mathbf{e}_2\quad\mathbf{e}_3)\begin{pmatrix}a_1 & 0\\ 0 & a_2\\ 0 & 0\end{pmatrix}\begin{pmatrix}\mathbf{u}_1^T\\ \mathbf{u}_2^T\end{pmatrix}, \tag{16}$$

where R is a 3×3 orthogonal matrix whose orthonormal three column vectors are $\mathbf{e}_1$, $\mathbf{e}_2$, and $\mathbf{e}_3$, and U is a 2×2 orthogonal matrix whose orthonormal two column vectors are $\mathbf{u}_1$ and $\mathbf{u}_2$. N is a 3×2 diagonal matrix whose diagonal elements a_1 and a_2 are called the singular values of W_s and off-diagonal elements are all equal to zero. All of the singular values and unit vectors in Eq. (16) must satisfy the following eigenvalue problems:[32]

$$(W_sW_s^T)\mathbf{e}_\alpha=a_\alpha^2\mathbf{e}_\alpha\quad(\alpha=1,2,3), \tag{17}$$

$$(W_s^TW_s)\mathbf{u}_\beta=a_\beta^2\mathbf{u}_\beta\quad(\beta=1,2), \tag{18}$$

respectively. Two of the eigenvalues of $W_sW_s^T$ and the eigenvalues of $W_s^TW_s$ are equal to the square of singular values, a_1^2 and a_2^2. We set the order $a_1\geqslant a_2$. The eigenvectors $\mathbf{e}_1$, $\mathbf{e}_2$, and $\mathbf{e}_3$ coincide with the principal axes of the instantaneous moment of inertia tensor of the triatomic system, since the off-diagonal elements of moment of inertia tensor Eq. (6) coincide with those of the matrix $W_sW_s^T$ except for their sign. In our triatomic system, the third eigenvalue of $W_sW_s^T$, a_3^2, is zero and the corresponding eigenvector is set to be $\mathbf{e}_3=(0,0,1)^T$. That is, the system is planar and always laid on the *x*-*y* plane. At the same time, *z* components of $\mathbf{e}_1$ and $\mathbf{e}_2$ are always zero. We restrict both R and U to be a proper rotation matrix. These are parametrized by θ and φ respectively. φ is referred to as the hyperangle. To summarize, Eq. (15) is made explicit in terms of these quantities as

$$W_s=\begin{pmatrix}\cos\theta & -\sin\theta & 0\\ \sin\theta & \cos\theta & 0\\ 0 & 0 & 1\end{pmatrix}\begin{pmatrix}a_1 & 0\\ 0 & a_2\\ 0 & 0\end{pmatrix}\times\begin{pmatrix}\cos\varphi & \sin\varphi\\ -\sin\varphi & \cos\varphi\end{pmatrix}. \tag{19}$$

In PAHC's the left-most matrix R in the right-hand side of Eq. (15) identifies a body frame (the principal-axis frame). The Jacobi vectors referred to this body frame, $\boldsymbol{\rho}_1$ and $\boldsymbol{\rho}_2$, are expressed as [cf. Eq. (2)]

$$(\boldsymbol{\rho}_1\quad\boldsymbol{\rho}_2)=NU^T=\begin{pmatrix}a_1\cos\varphi & a_1\sin\varphi\\ -a_2\sin\varphi & a_2\cos\varphi\\ 0 & 0\end{pmatrix}. \tag{20}$$

Thus the three-dimensional internal space is composed of the variables a_1, a_2, and φ. The singular values a_1 and a_2 are called "gyration radii,"[27] since they represent the mass-weighted length (size) of the system along each principal axis. We let the sign of a_2 classify the permutational isomers of the triatomic cluster.[33] That is, if $\hat{\mathbf{z}}\cdot(\boldsymbol{\rho}_{s1}\times\boldsymbol{\rho}_{s2})>0$, which is the case for the structure of type (A) in Fig. 1, a_2 is positive. Otherwise [type (B) in Fig. 1], a_2 is negative, where $\hat{\mathbf{z}}$ is a unit vector along the positive *z* axis. Condition $a_2=0$ specifies a collinear molecular shape.

In Eq. (19), the angle θ specifies the orientation of the principal-axis frame of the three-atom molecule and has nothing to do with the shape of the molecule. The continuous change in θ causes the ordinary rotation of the system. On the other hand, the continuous change in φ in Eq. (19), which is called the kinematic or democratic rotation, generally brings about a change in molecular shape exchanging the positions of the constituent atoms in a democratic manner. It is proved[33] that the range of the hyperangle φ is limited to $0 \leqslant \varphi < \pi$ for φ to preserve a one-to-one correspondence between the molecular shape and the internal coordinates.

D. Classical equations of motion

In the internal space defined above, we consider the classical equations of motion in terms of the PAHC's. Applying Eq. (20) to Eq. (6), we obtain for the moment of inertia tensor referred to the body frame as

$$M = \begin{pmatrix} a_2^2 & 0 & 0 \\ 0 & a_1^2 & 0 \\ 0 & 0 & a_1^2 + a_2^2 \end{pmatrix}, \tag{21}$$

which is diagonal as is expected. From Eqs. (21) and (20), the gauge potential Eq. (7) is calculated for the internal coordinates to be

$$\mathbf{A}_{a_1} = \mathbf{0}, \quad \mathbf{A}_{a_2} = \mathbf{0}, \quad \mathbf{A}_{\varphi} = \begin{pmatrix} 0 \\ 0 \\ -\dfrac{2a_1 a_2}{a_1^2 + a_2^2} \end{pmatrix}. \tag{22}$$

Since the pseudometric tensor $h_{\mu\nu}$ defined in Eq. (9) for the coordinates (a_1, a_2, φ) becomes

$$(h_{\mu\nu}) = \begin{pmatrix} 1 & 0 & 0 \\ 0 & 1 & 0 \\ 0 & 0 & a_1^2 + a_2^2 \end{pmatrix}, \tag{23}$$

in a matrix form, we obtain the true metric tensor $g_{\mu\nu}$ as

$$(g_{\mu\nu}) = \begin{pmatrix} 1 & 0 & 0 \\ 0 & 1 & 0 \\ 0 & 0 & \dfrac{(a_1^2 - a_2^2)^2}{a_1^2 + a_2^2} \end{pmatrix} \tag{24}$$

by applying Eqs. (21)–(23) to Eq. (11). Thus a subspace composed of the gyration radii a_1 and a_2 is Euclidean, since $g_{11} = g_{22} = 1$ and $g_{12} = g_{21} = 0$. We call this Euclidean space "gyration space," where the hyperangle φ is kept constant.

With use of this gauge-invariant metric tensor $g_{\mu\nu}$, the Lagrangian for the triatomic system of vanishing angular momentum is given as

$$\mathcal{L} = \frac{1}{2}\left\{ \dot{a}_1^2 + \dot{a}_2^2 + \frac{(a_1^2 - a_2^2)^2}{a_1^2 + a_2^2}\dot{\varphi}^2 \right\} - V(a_1, a_2, \varphi). \tag{25}$$

Subsequently, the classical equations of motion are obtained as

$$\ddot{a}_1 = \frac{a_1(a_1^2 + 3a_2^2)(a_1^2 - a_2^2)}{(a_1^2 + a_2^2)^2}\dot{\varphi}^2 - \frac{\partial V}{\partial a_1}, \tag{26}$$

$$\ddot{a}_2 = \frac{a_2(a_2^2 + 3a_1^2)(a_2^2 - a_1^2)}{(a_1^2 + a_2^2)^2}\dot{\varphi}^2 - \frac{\partial V}{\partial a_2}, \tag{27}$$

and

$$\frac{d}{dt} L_D = -\frac{\partial V}{\partial \varphi}, \tag{28}$$

where we have defined the democratic angular momentum L_D as

$$L_D \equiv \frac{\partial \mathcal{L}}{\partial \dot{\varphi}} = \frac{(a_1^2 - a_2^2)^2}{a_1^2 + a_2^2}\dot{\varphi}. \tag{29}$$

L_D is an angular momentum of the democratic rotation and is a constant of motion along a geodesic in the internal space.

We note that a kind of "centrifugal force" is generated in the gyration space as seen in the first terms on the right-hand sides of Eqs. (26) and (27), which are proportional to the square of angular velocity of the democratic rotation $\dot{\varphi}$. We call this force "democratic centrifugal force (DCF)." DCF is different from the ordinary centrifugal force, and it is not zero even in case of zero angular momentum. Figure 2 shows an example of the field of DCF on gyration space for a selected $\dot{\varphi}$. It can be seen that the DCF works so as to avoid the degeneracy of the two gyration radii, $a_1 = |a_2|$. The arrows in Fig. 2 tend to align parallel to the positive a_1 axis for large a_1 with small $|a_2|$. These characteristics of the DCF indicate that an isolated triatomic system intrinsically tends to be longer in the longer direction and to be shorter in the shorter direction along the principal axes. (Here, the terms longer and shorter are in the meaning of the gyration radii.) Notice that this effect of the DCF is a purely kinematic one and can compete with the potential force as is expected from Eqs. (26) and (27). We will scrutinize this point later.

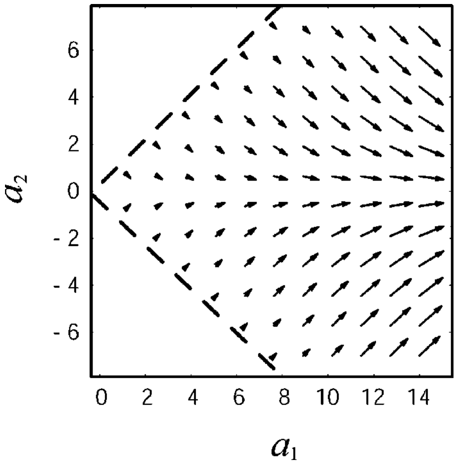

FIG. 2. The field of the democratic centrifugal force (DCF) on the gyration space at a typical value of $\dot{\varphi}$. The broken lines represent degeneracy between the two gyration radii, $a_1 = |a_2|$.

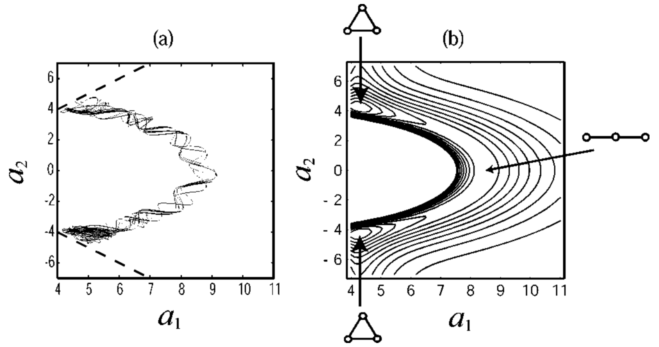

FIG. 3. (a) A trajectory on gyration space corresponding to the time evolution in Fig. 4. The broken lines are the degeneracy lines between the two gyration radii, $a_1 = |a_2|$. (b) Potential-energy surface on gyration space with hyperangle φ fixed to 0 or $\pi/3$ or $2\pi/3$. The permutationally distinct local equilibrium structures (equilateral triangles) are located at (4.24,4.24) and (4.24,−4.24), where the potential energy is $V = -3.00\varepsilon$, and the collinear transition state is located at (8.48,0), where the potential energy is $V = -2.005\varepsilon$. The energy difference between the neighboring contour lines is 0.231ε.

III. RECROSSING MOTION AROUND THE TRANSITION STATE DUE TO DEMOCRATIC CENTRIFUGAL FORCE—A UNIFIED VIEW

A. Potential topography in internal space and reaction path

To analyze the mechanism of the isomerization dynamics, we now map the potential function and dynamics onto appropriate subspaces of the internal space. First of all, the two local equilibrium structures (equilateral triangle) are at $(a_1, a_2) = (4.24, \pm 4.24)$, where the sign of a_2 characterizes the two permutational isomers as we have defined in Sec. II C, whereas those for the collinear saddle structures are $(a_1, a_2) = (8.48, 0)$. Figure 3(b) shows the potential-energy surface mapped on the gyration space (a_1, a_2) with hyperangle φ fixed to 0 or $\pi/3$ or $2\pi/3$. The topography of the potential-energy surface is exactly common to these three angles for φ as a result of permutational symmetry. A typical trajectory above the isomerization threshold is also mapped onto this space as shown in Fig. 3(a), which outlines a reaction path of the isomerization.

To see the dynamics of this trajectory in the entire internal space (a_1, a_2, φ), we plot the time series of these variables in Fig. 4. In this particular example, the trajectory crosses the collinear configuration $|a_2| = 0$ five times. On the other hand, φ is almost "locked" to 0 or $\pi/3$ or $2\pi/3$ with small and rapid oscillations during such an isomerization dynamics. Note that $\varphi = 0$ and $\varphi = \pi$ are connected since φ is π periodic. Substituting the three angles about which φ is locked into Eq. (20), one confirms that they characterize the three permutationally distinct oblate isosceles triangle structures of the M_3 cluster. Therefore the locking phenomenon of the hyperangle during the isomerizing motions indicates that the cluster undergoes isomerization mostly keeping the isosceles-triangle symmetry. Thus φ classifies the reaction channels. The correspondence between the angles of φ and the reaction channels is shown in Fig. 1.

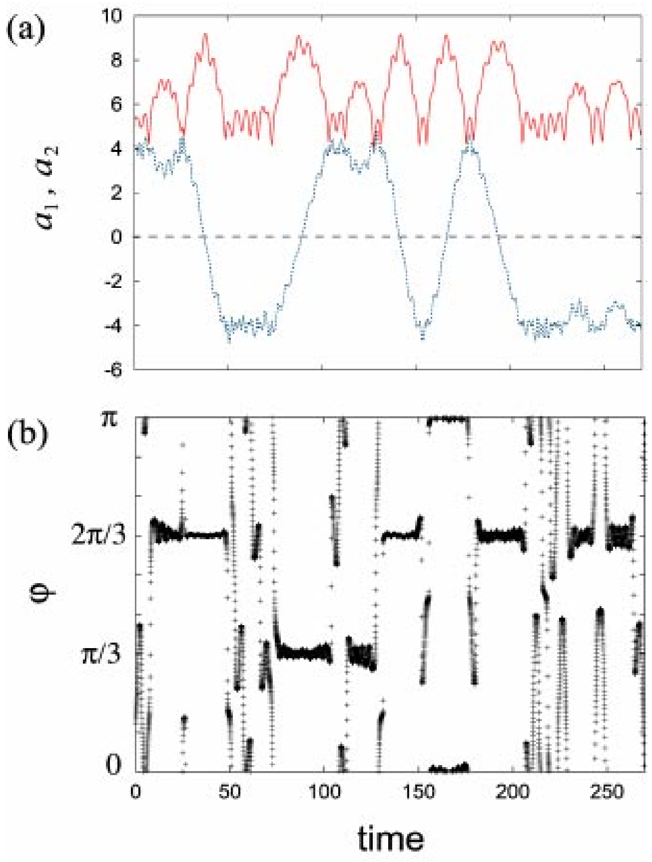

FIG. 4. A typical time series of the two gyration radii, a_1 and a_2 ($a_1 \geqslant a_2$), and the hyperangle φ in triatomic Morse cluster M_3 at the total energy $E = -1.60\varepsilon$. The condition $a_2 = 0$ (indicated by the horizontal broken line) represents the collinear configurations. During this period, the saddle crossing has taken place five times. The locked angle $\varphi = 0$, $\pi/3$, $2\pi/3$ specifies the three permutationally distinct saddle structures.

The reason why the hyperangle is locked to the vicinity of 0 or $\pi/3$ or $2\pi/3$ during the isomerization dynamics is comprehended as follows. In Figs. 5(a) and 5(b), the potential-energy surfaces on the gyration space with the hyperangle φ slightly shifted (by $\pi/30$ and $\pi/12$) from 0 or $\pi/3$ or $2\pi/3$ are shown. These figures show that the height of potential barrier along the reaction path rapidly increases and the reaction channel is quickly closed when φ is shifted from

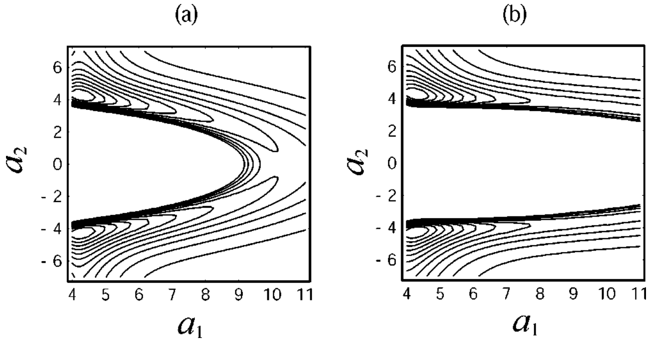

FIG. 5. Potential-energy surfaces $V(a_1, a_2, \varphi)$ mapped onto the gyration space. The hyperangle is fixed to (a) $\varphi = (0 \text{ or } \pi/3 \text{ or } 2\pi/3) + \pi/30$, and (b) $\varphi = (0 \text{ or } \pi/3 \text{ or } 2\pi/3) + \pi/12$. The potential energy at (4.24,±4.24) is -3.00ε in both figures. The energy difference between the neighboring contour lines is 0.231ε.

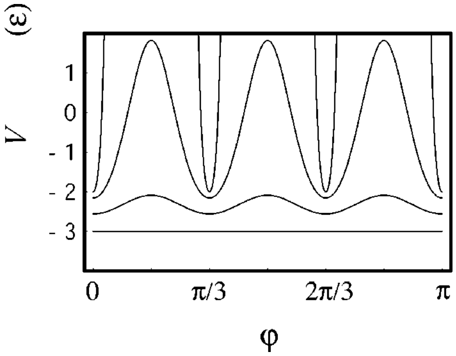

FIG. 6. Potential-energy curves against the hyperangle φ with the gyration radii a_1 and a_2 fixed to $(a_1,a_2)=(4.24,4.24)$, (5.0,3.9), (6.0,3.5), (8.48,0) from the bottom to the top. These values for gyration radii are selected along the reaction coordinate in Fig. 3(b).

0 or $\pi/3$ or $2\pi/3$. In this sense, the hyperangle φ plays a role of gating the reaction path on the gyration space.

On the other hand, the stability of locking of φ can be understood in terms of the potential energy against φ. Figure 6 shows the potential profiles for four given sets of gyration radii, $(a_1,a_2)=(4.24,4.24)$, (5.0,3.9), (6.0,3.5), (8.48,0), which are picked up along the reaction path in Fig. 3. The potential curve with respect to φ is flat for a trajectory that is in the vicinity of the equilibrium configuration $(a_1,a_2)=(4.24,4.24)$, where a large and rapid democratic rotation is possible. The potential curve begins to swell as the gyration radii recedes from the equilibrium, and near the collinear transition state $(a_1,a_2)=(8.48,0)$, only the regions around 0 or $\pi/3$ or $2\pi/3$ for φ are energetically accessible. Therefore the locking of hyperangle tends to become tighter as the system climbs up the reaction path on the gyration space.

Based on the above observations, reaction mechanism of M_3 cluster can be summarized as follows. In the motions around the local equilibrium structure, a trajectory on the gyration space searches for a chance to get into the reaction path, the switch of which is turned on and off frequently due to the rapid democratic rotation. In this regime, dynamics of the cluster is dominated by all of the three internal variables, a_1, a_2, and φ. Once a trajectory on the gyration space becomes successful to get into the reaction path, the hyperangle is locked tightly so as to allow the trajectory to pass through the transition state. Thus the two variables, a_1 and a_2, play a role of the collective coordinates.

B. Precise role of the democratic centrifugal force

We proceed to more precise study of the effects of the democratic centrifugal force (DCF). As can be seen from Fig. 4, φ generally varies rapidly in the vicinity of the local equilibrium points. The origin of this rapid democratic rotation can be understood by expressing $\dot{\varphi}$ explicitly as

$$\dot{\varphi}=\dot{\mathbf{u}}_1\cdot\mathbf{u}_2=\frac{\mathbf{u}_1^T(\dot{W}_s^T W_s+W_s^T\dot{W}_s)\mathbf{u}_2}{a_1^2-a_2^2}, \tag{30}$$

which is obtained by differentiating Eq. (18) for $\beta=1$ with respect to time and taking scalar product with $\mathbf{u}_2$. Since the numerator of Eq. (30) is generally not zero, very rapid democratic rotation occurs as a_1 and $|a_2|$ come close to each other and $\dot{\varphi}$ can even diverge. Inserting Eq. (30) into the components of DCF in Eqs. (26) and (27) shows that in such a case, both $\ddot{a}_1$ and $\ddot{a}_2$ can diverge. Therefore the very rapid democratic rotation near the line of degeneracy, $a_1=|a_2|$ (see Fig. 2) necessarily generates a very strong DCF so as to avoid the complete degeneracy. In order to confirm this effect more quantitatively, we show in Fig. 7 a frequency distribution of $a_1-|a_2|$ in many classical trajectories whose total internal energy is below the isomerization threshold. It is evident that the trajectories tend to avoid the vicinity of the degeneracy region, which in turn implies that the triatomic cluster tends to be in an unsymmetrical mass balance. Since the directionality of DCF field in Fig. 2 and the direction of the reaction path in Fig. 3(b) are nearly parallel to each other except for the saddle region, the DCF will help trajectories to climb up the hill along the reaction path in the gyration space.

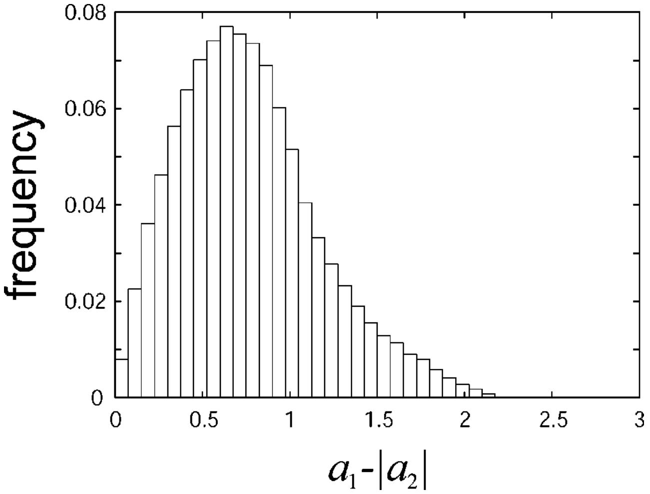

FIG. 7. Frequency distribution for the difference between the two gyration radii, $a_1-|a_2|$, sampled from classical trajectories whose total internal energy is $E=-2.2\varepsilon$ (normalized to unity).

The effect of DCF that induces asymmetry in the mass balance becomes more prominent in the vicinity of the transition state. Although the hyperangle φ is locked around 0 or $\pi/3$ or $2\pi/3$ during the isomerizing motions, it oscillates within a small range around these angles (see Fig. 4). This oscillation brings about a remarkable effect that is as significant as the potential force. It should be recalled that the DCF tends to be stronger in the vicinity of the transition states than in that of the equilateral triangle structures for a common value of $\dot{\varphi}$, which is demonstrated by the length of the arrows in Fig. 2. Notice that the arrows in Fig. 2 are directed to the line $a_2=0$ (dividing line or the collinear transition state) from both sides, resulting in a tendency to be parallel to this line around it. This suggests that the DCF should have an effect of trapping trajectories in the vicinity of the collinear saddle structure. In fact, such tentatively trapped trajectories are frequently observed even at a relatively high internal energy. A typical example of the time evolution of gyration radii for the trapped motion is shown in Fig. 8(a). In this figure, the gyration radii a_1 and a_2 keep close to the values of the collinear saddle structure $(a_1,a_2)=(8.48,0)$ for a long time before falling to one of the regions of equi-

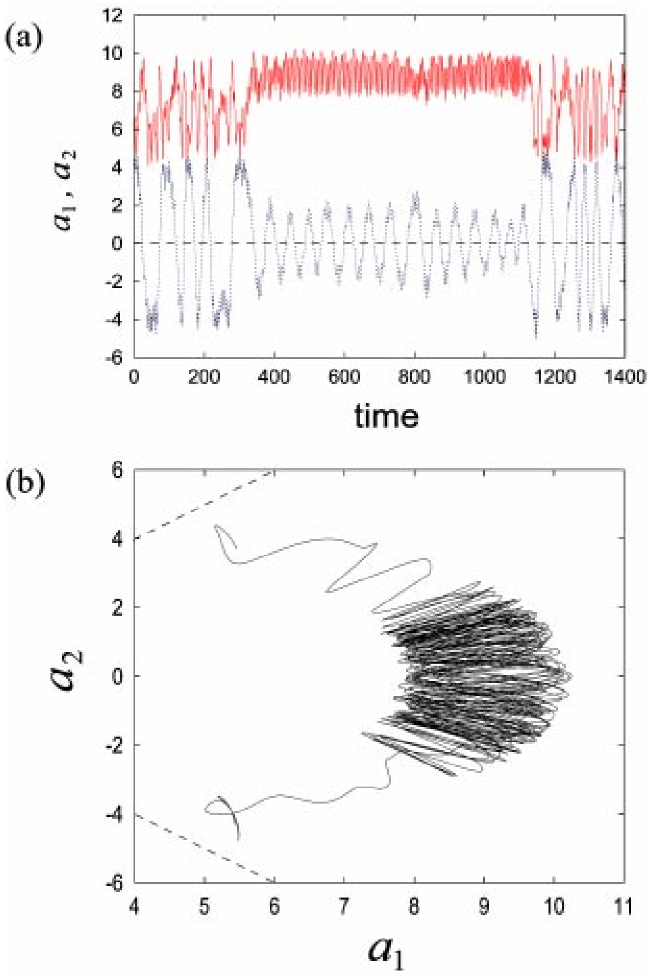

FIG. 8. (a) A typical time evolution of gyration radii, a_1 and a_2 ($a_1 \geqslant a_2$), which shows a "trapped" motion in the vicinity of the collinear saddle structure from $t \approx 350$ to $t \approx 1100$ recrossing the so-called "dividing surface" many times. Total internal energy of the trajectory is $E = -1.16\varepsilon$. (b) The corresponding trajectory on the gyration space from $t = 314$ to $t = 1147$ in (a).

librium structures $[(a_1, a_2) = (4.24, \pm 4.24)]$. Figure 8(b) shows the corresponding trajectory on the gyration space in the interval $t = 314 \sim t = 1147$ in Fig. 8(a). It oscillates in the direction of not only a_1 (corresponding to symmetric and antisymmetric stretching motions) but also a_2 (bending motion).

It is obvious that the saddle structure of the potential topography alone [see Fig. 3(b)] cannot support the trapping motion. To comprehend the total effects arising from both the bear potential surface and the DCF, we superimpose these factors appearing in the Lagrangian Eq. (25) into the form of an effective potential such that

$$V_{\mathrm{eff}} \equiv -\frac{1}{2} \frac{(a_1^2 - a_2^2)^2}{a_1^2 + a_2^2} \dot{\varphi}^2 + V(a_1, a_2, \varphi). \tag{31}$$

The resultant topography of V_{eff} is shown in Fig. 9, where φ is set to 0 or $\pi/3$ or $2\pi/3$ and $|\dot{\varphi}| = 0.05$, which is a roughly averaged value during the period of the trapped motions. It clearly demonstrates that a basin does appear now around the saddle region of the potential-energy surface. The larger $\dot{\varphi}$ forms the wider and deeper basin in general.

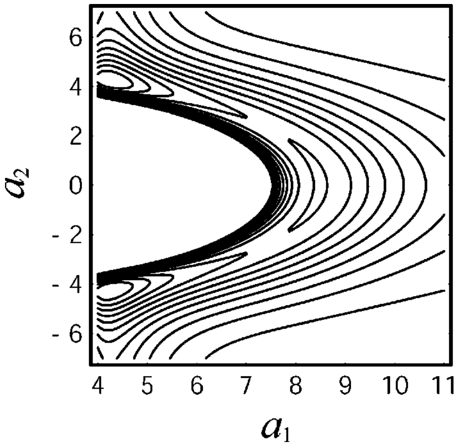

FIG. 9. The effective potential-energy surface, Eq. (31), mapped onto the gyration space. The hyperangle φ is fixed to 0 or $\pi/3$ or $2\pi/3$. The democratic angular velocity is set to $|\dot{\varphi}| = 0.05$. The energy difference between the neighboring contour lines is 0.231ε.

Trapped motion in the vicinity of a transition state in three atomic chemical reactions such as $H + H_2$ has been discussed in the literature for decades. This is because the trapping motion is regarded as one of the main factors that bring about the overestimate of reaction rate in the transition state theory. Most of the past studies have focused on the resonant motion on the skewed potential surfaces for the collinear configuration.[37,38] On the other hand, the present approach has identified the kinematic origin of the trapped motions that accounts for trapping not only within the collinear configuration but also in the direction of bendinglike motion out of the collinear configuration.

Our approach also provides a new insight into the regularity of the dynamics around the saddle region in van der Waals clusters, which has been discussed for a decade.[4,5] It is widely recognized through numerical investigations that the dynamics in the saddle region are generally more regular than that in the bottom region. This can be rationalized quite naturally from our point of view: First, the effective degrees of freedom that dominate the saddle-crossing motion are reduced from three (a_1, a_2, φ) in the bottom region to two (a_1, a_2) due to the locking of the hyperangle φ. Second, the basin structure thus found should help to reduce the irregular (chaotic) behavior. Thus, in our view, the stability of motion in the vicinity of transition state is a result of the fact that the transition state is coincidentally located on the *focal line* of the DCF, that is, on the line $a_2 = 0$ on the gyration space.

IV. EFFECTS OF THE GAUGE FIELD ASSOCIATED WITH THE ECKART FRAME AS A SUPPRESSING FACTOR OF ISOMERIZATION

We now quantify how much the existence of the gauge field $\{\mathbf{A}_\mu\}$ in internal space (or correspondingly the movements of the associated body frame under zero total angular momentum) may contribute to the reaction rate by comparing two dynamics; one which is equipped with the full effects of the gauge field (true dynamics) as studied above and the other in which the gauge-field effect is eliminated. As a typical example of the eliminated gauge field in the latter dynamics, we choose the one associated with the so-called Eckart frame[16–19] and with the normal-mode coordinates. In case of the large-amplitude motions like isomerization reactions, the effect of the gauge field is never negligible and should be studied in a quantitative manner. The standard classical trajectory simulations of molecular dynamics quite often do not care about the existence of the gauge field in the $(3n-6)$-dimensional internal space, since they are usually carried out in the $(3n-3)$-dimensional Jacobi coordinate scheme (or even in the $3n$-dimensional original Cartesian space for a very large system) and its orthogonally transformed variants. Nevertheless, such a comparison should be meaningful in that the gauge-field effect is made quantitatively explicit. To our best knowledge, no report has been made before about the actual quantitative effect arising from the curved nature of molecular internal space induced by the gauge fields, although considerable studies on theoretical formulation have been made in the literature. Also, we are concerned with a fact that the conventional theories of chemical reaction are often constructed based on the tentative separation of rotational and internal motions using the Eckart frame and disregarding the effects of the gauge field. For example, the rotational and vibrational partition functions that arise in the rate expression are often calculated based on the rigid-body approximation and the normal-mode frequencies, respectively.[7] Hence we should clarify how much such an effect of the gauge field can contribute to the reaction rate.

A. Eckart subspace and Eckart frame

In this subsection, we consider an n-atom system in three-dimensional space for generality. Let the $n-1$ three-dimensional vectors $\{\mathbf{z}_{si}\}\,(i=1,...,n-1)$ be the mass-weighted Jacobi vectors for a reference molecular configuration. The reference configuration is usually set to be a local equilibrium structure of the molecule oriented to a certain direction. The Eckart subspace is defined as a $(3n-6)$-dimensional subspace in the $(3n-3)$-dimensional translation-reduced configuration space $\{\boldsymbol{\rho}_i^E\}\,(i=1,...,n-1)$ with three additional constraint conditions called the Eckart conditions,

$$\sum_{i=1}^{n-1} \boldsymbol{\rho}_i^E \times \mathbf{z}_{si} = \mathbf{0}. \tag{32}$$

The geometrical meaning is that the Eckart subspace $\{\boldsymbol{\rho}_i^E\}$ is perpendicular to the three-dimensional manifold of rigid-body rotation at the reference configuration $\{\mathbf{z}_{si}\}$. The Eckart subspace is Euclidean, since the conditions in Eq. (32) are linear. Therefore this space can be spanned by vectors $\{\mathbf{n}_{i\mu}\}\,(\mu=1,...,3n-6)$ which specify the $3n-6$ directions of vibrational normal modes at the reference configuration $\{\mathbf{z}_{si}\}$ in the $(3n-3)$-dimensional configuration space. The vectors $\{\mathbf{n}_{i\mu}\}$ are also perpendicular to the rotation manifold at $\{\mathbf{z}_{si}\}$ and thereby satisfy the conditions

$$\sum_{i=1}^{n-1} \mathbf{n}_{i\mu} \times \mathbf{z}_{si} = 0 \tag{33}$$

together with the orthonormal conditions

$$\sum_{i=1}^{n-1} \mathbf{n}_{i\mu} \cdot \mathbf{n}_{i\nu} = \delta_{\mu\nu}. \tag{34}$$

Thus the Eckart subspace can be parametrized by the $3n-6$ internal coordinates $\{q^\mu\}$ as

$$\boldsymbol{\rho}_i^E(\{q^\mu\}) = \mathbf{z}_{si} + \sum_{\mu=1}^{3n-6} \mathbf{n}_{i\mu} q^\mu. \tag{35}$$

The Eckart frame with respect to the reference configuration $\{\mathbf{z}_{si}\}$ for an arbitrary configuration $\{\boldsymbol{\rho}_{si}\}$ is given by a proper rotation $R \in \mathrm{SO}(3)$ that satisfies

$$\sum_{i=1}^{n-1} (R^T \boldsymbol{\rho}_{si}) \times \mathbf{z}_{si} = \mathbf{0}. \tag{36}$$

We call the gauge convention that refers to the Eckart frame the "Eckart gauge." In general, the reference configuration $\{\mathbf{z}_{si}\}$ in Eq. (32) does not have to be a local equilibrium structure. For instance, it can be set at a point along a trajectory as in the instantaneous normal-mode analysis[5] and along a reaction coordinate in the theory of the reaction path Hamiltonian.[20] For our analysis of the M_3 cluster, we set the reference configuration so as to be the equilibrium equilateral triangle structure [type (A) in Fig. 1], in which its two Jacobi vectors $\mathbf{z}_{s1}$ and $\mathbf{z}_{s2}$ are parallel to the x and y axis of the space-fixed frame, respectively.

It is essential in the Eckart gauge that the gauge potential $\mathbf{A}_\mu$ in Eq. (7) vanishes at the reference configuration as

$$\mathbf{A}_\mu = M^{-1} \sum_{i=1}^{n-1} \mathbf{z}_{si} \times \mathbf{n}_{i\mu} = \mathbf{0}, \tag{37}$$

where we have inserted Eq. (35) into Eq. (7) and set $\{q^\mu\} = \{0\}$ in the first equality, and used Eq. (33) in the second equality. Therefore the pseudometric $h_{\mu\nu}$ here can be a good approximation to $g_{\mu\nu}$ as far as a small-amplitude vibration around the reference configuration is concerned. Furthermore, the resultant $h_{\mu\nu}$ becomes simply Euclidean, $h_{\mu\nu} = \delta_{\mu\nu}$, for the normal-mode coordinates $\{q^\mu\}$. Thus the classical equations of internal motion disregarding the gauge field are given as the familiar looking Newtonian equations

$$\ddot{q}^\mu = -\frac{\partial V}{\partial q^\mu}. \tag{38}$$

Since the pseudometric $h_{\mu\nu}$ in the Eckart gauge is the metric of the Eckart subspace by definition [cf. Eq. (9)], the confined motion to the Eckart subspace obeys the same equation as Eq. (38). Thus the Eckart subspace can be approximately identified to be the molecular internal space. However, even if the total angular momentum is zero, a trajectory starting from a point on the Eckart subspace gradually gets away from the subspace and wanders widely in the entire $(3n-3)$-dimensional translation-reduced configuration space. The "falling cat" phenomenon never takes place as long as the dynamics is confined to the Eckart subspace since the

Eckart frame is fixed. Thus Eq. (38) is never rigorous and therefore it is quite important to quantify how large an error can result.

The rigorous dynamics in the internal space can be represented even in terms of the normal-mode coordinate system by taking an appropriate account of the true metric $g_{\mu\nu}$ in Eq. (11). Since $h_{\mu\nu}=\delta_{\mu\nu}$ holds in the Eckart gauge, Eq. (11) is written as

$$g_{\mu\nu}=\delta_{\mu\nu}-\mathbf{A}_\mu^T M \mathbf{A}_\nu, \tag{39}$$

where the moment of inertia tensor M and the gauge potential $\{\mathbf{A}_\mu\}$ are those referred to the Eckart frame defined as Eqs. (6) and (7), respectively. Although the components of the gauge potential are small in the vicinity of the reference configuration, they generally do not vanish except there,[25] and the true metric $g_{\mu\nu}$ is no longer Euclidean due to the second term in the right-hand side of Eq. (39). The rigorous equations of motion (for zero angular momentum) are thus obtained as

$$g_{\mu\nu}(\ddot{q}^\nu+\Gamma^\nu_{\kappa\lambda}\dot{q}^\kappa\dot{q}^\lambda)=-\frac{\partial V}{\partial q^\mu}, \tag{40}$$

where the Christoffel symbols $\Gamma^\nu_{\kappa\lambda}$ are defined by

$$\Gamma^\nu_{\kappa\lambda}=\frac{1}{2}g^{\nu\mu}\left(\frac{\partial g_{\mu\kappa}}{\partial q^\lambda}+\frac{\partial g_{\mu\lambda}}{\partial q^\kappa}-\frac{\partial g_{\kappa\lambda}}{\partial q^\mu}\right). \tag{41}$$

The dynamics arising from these equations of motion should be compared with the dynamics of Eq. (38) under no gauge field.

B. Effects of the gauge field on isomerization reactions: A numerical experiment

We study the rate of isomerization of the M_3 cluster. To do so, we run 5000 trajectories of an internal energy $E=-1.6\varepsilon$, which is above the isomerization threshold. Random sampling to prepare the initial conditions in configuration space are made so as to set them to be common to the two different dynamics [Eqs. (40) and (38)]. It is not a straightforward matter to judge whether a trajectory starting from one potential basin has moved to the other accomplishing a reaction, since it generally undergoes recrossing over the dividing surface and the reaction does not end up with dissociation (having no asymptotic region to mark the end). Here in this particular case study we monitor the time-dependent number of trajectories that remain in the original basin (Fig. 10). Practically, a trajectory is discarded from the set of surviving trajectories as soon as it passes across the dividing surface along the collinear configuration, and the recrossing motion is simply disregarded. The mean first passage time, that is, an average time for the trajectories to arrive at the dividing surface is also measured (Fig. 11).

Figure 10 shows the decay in the number of such surviving trajectories of the M_3 isomers of type (A) in Fig. 1. Since the survival number decays mostly in an exponential manner in the both dynamics, they must be sufficiently stochastic. (The absence of decay in the very short time range is due to the specific initial conditions that all atoms are at rest.) From the figure, it is clear that the decay of the survival number has been significantly suppressed by the gauge field. Figure 11 demonstrates that the suppression can be seen in a wide range of the internal energy. The difference between the mean first passage times in these dynamics amounts to about 20–30%, which is far beyond a negligible quantity. These results strongly suggest that one may *overestimate* the reaction rate of the structural isomerization to such a large value by disregarding the effects of the gauge field in the internal space.

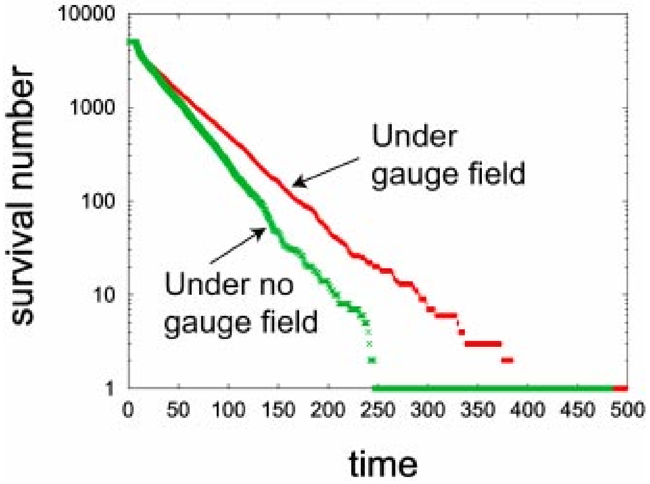

FIG. 10. Decay of the number of surviving trajectories of the M_3 against isomerization (see the text for the precise definition of "isomerization"). The lower curve represents the dynamics without the gauge-field effect, Eq. (38), while the upper one indicates the true dynamics under the full gauge field, Eq. (40). All of the initial conditions are randomly sampled in configuration space and are taken to be exactly the same for the two sets of dynamics. Number of the sample trajectories is 5000 and their internal energy is set to $E=-1.6\varepsilon$.

C. Mechanism of suppressing the reaction rate

The principal-axis hyperspherical coordinates (PAHC's) turned out to be so nice a coordinate system for understand-

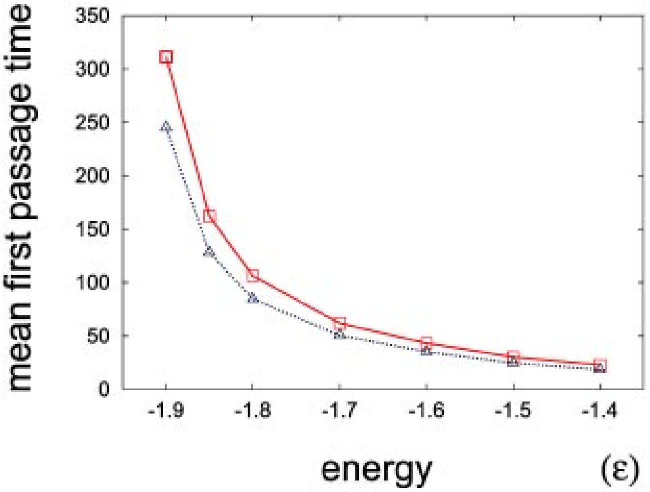

FIG. 11. Internal-energy dependence of mean first passage time (average lifetime) of the M_3 cluster. The lower curve represents the dynamics under no gauge field, Eq. (38), while the upper one shows the data for the true dynamics, Eq. (40).

ing the mechanism of the structural isomerization of the M_3 cluster as seen in Sec. III that we here analyze the dynamics without the gauge field in terms of the PAHC's. Recently, Littlejohn *et al.*[33] have presented an explicit parametrization of the Eckart subspace in terms of the PAHC's (a_1, a_2, φ) for three-atom systems whose reference configuration is the same as ours defined in Sec. IV A. The result is expressed as

$$(\boldsymbol{\rho}_1^E \quad \boldsymbol{\rho}_2^E) = \begin{pmatrix} \cos\varphi & -\sin\varphi & 0 \\ \sin\varphi & \cos\varphi & 0 \\ 0 & 0 & 1 \end{pmatrix} \begin{pmatrix} a_1 & 0 \\ 0 & a_2 \\ 0 & 0 \end{pmatrix} \begin{pmatrix} \cos\varphi & \sin\varphi \\ -\sin\varphi & \cos\varphi \end{pmatrix} \tag{42}$$

$$= \begin{pmatrix} a_1\cos^2\varphi + a_2\sin^2\varphi & (a_1 - a_2)\sin\varphi\cos\varphi \\ (a_1 - a_2)\sin\varphi\cos\varphi & a_1\sin^2\varphi + a_2\cos^2\varphi \\ 0 & 0 \end{pmatrix}. \tag{43}$$

With this parametrization and Eq. (9), the pseudometric tensor $h_{\mu\nu}$ of the Eckart subspace is represented as

$$(h_{\mu\nu}) = \begin{pmatrix} 1 & 0 & 0 \\ 0 & 1 & 0 \\ 0 & 0 & 2(a_1 - a_2)^2 \end{pmatrix}. \tag{44}$$

Then the associated Lagrangian for the dynamics without the gauge field turns out to be

$$\mathcal{L} = \frac{1}{2}\{\dot{a}_1^2 + \dot{a}_2^2 + 2(a_1 - a_2)^2\dot{\varphi}^2\} - V(a_1, a_2, \varphi), \tag{45}$$

and the classical equations of motion are

$$\ddot{a}_1 = 2(a_1 - a_2)\dot{\varphi}^2 - \frac{\partial V}{\partial a_1}, \tag{46}$$

$$\ddot{a}_2 = 2(a_2 - a_1)\dot{\varphi}^2 - \frac{\partial V}{\partial a_2}, \tag{47}$$

$$\frac{d}{dt}[2(a_1 - a_2)^2\dot{\varphi}] = -\frac{\partial V}{\partial \varphi}. \tag{48}$$

Comparing these expressions with Eqs. (26)–(28) directly gives a theoretical basis to see the consequence of neglecting the gauge-field effects. We see that the democratic centrifugal force (DCF) arises on the gyration space, but, in a different form. We now look into the details of the difference.

The field of the DCF in the dynamics without the gauge field in Eqs. (46) and (47) is shown in Fig. 12 at a selected $\dot{\varphi}$. Comparing Fig. 12 with Fig. 2, we see that the difference between these two force fields is most significant near the a_1 axis $(a_2 = 0)$, whereas it is small in the vicinity of the upper degeneracy line, $a_1 = a_2$. (Recall that we use only the upper-half plane, $a_2 \geqslant 0$, for the calculation of the reaction rate by definition.) In the true dynamics with the full gauge fields, the direction of the DCF lies more parallel to the a_1 axis in the vicinity of the dividing line $(a_2 = 0)$ than in the dynamics under no gauge field. In the dynamics without the gauge field, on the other hand, the DCF is always parallel to the line $a_1 = -a_2$ in the upper-half plane and tends to lead the molecular geometry to the collinear configuration, provided that a trajectory starts in the upper-half plane. But, at the same time, it keeps to push the trajectory carrying further across the dividing line in clear contrast to the true dynamics.

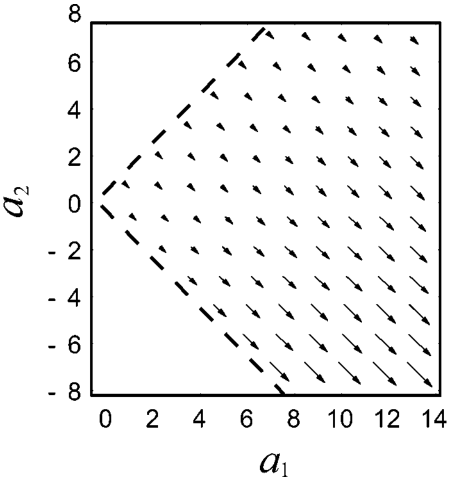

FIG. 12. The field of democratic centrifugal force on the gyration space arising from the dynamics under no gauge field. The length of each arrow reflects the strength of the force at each point for a given value of democratic angular velocity $\dot{\varphi}$. The broken lines are the degeneracy lines between the two gyration radii, $a_1 = |a_2|$.

In order to confirm the above-mentioned effect of the gauge field, we show in Fig. 13(a) the frequency distribution for the a_2 component of velocity vectors in the gyration space, $\dot{a}_2$, at the instant that the system crosses the line $a_2 = 0$ for these two dynamics. Note that $\dot{a}_2$ is directly related to the reactive flux at the dividing surface. It can be seen clearly in their difference [see Fig. 13(b)] that the dynamics under no gauge field has more components in the larger-$\dot{a}_2$ region. In fact, the average of them is $\langle \dot{a}_2 \rangle = 0.853$ and $\langle \dot{a}_2 \rangle = 0.910$ for the dynamics with and without the gauge field, respectively. This means that the trajectories getting out of the initial basin in the dynamics without the gauge field tend to be more *ballistic* and isomerization proceeds more smoothly. This proves the suppressing effect of the gauge field.

V. CONCLUDING REMARKS

We have clarified the nature of the internal motions of a triatomic cluster in terms of the principal-axis hyperspherical coordinates (PAHC's) based on a gauge-theoretical treatment. This coordinate system turned out to be quite effective both for understanding mechanism of the isomerization reaction and for extracting kinematic effects associated with the principal-axis frame. A collective reaction path has been extracted on a two-dimensional gyration space, since freezing of the hyperangle of the coordinates occurs during the isomerizing collective motions. Furthermore, we have obtained a kinematic force called democratic centrifugal force (DCF), which arises on the gyration space in response to the democratic rotation. It has been revealed that the DCF generally has an effect of inducing an asymmetry in mass balance of a system along principal axes and therefore the triatomic system tends to be collapsed towards the collinear shape, which helps the isomerization reaction to begin. A

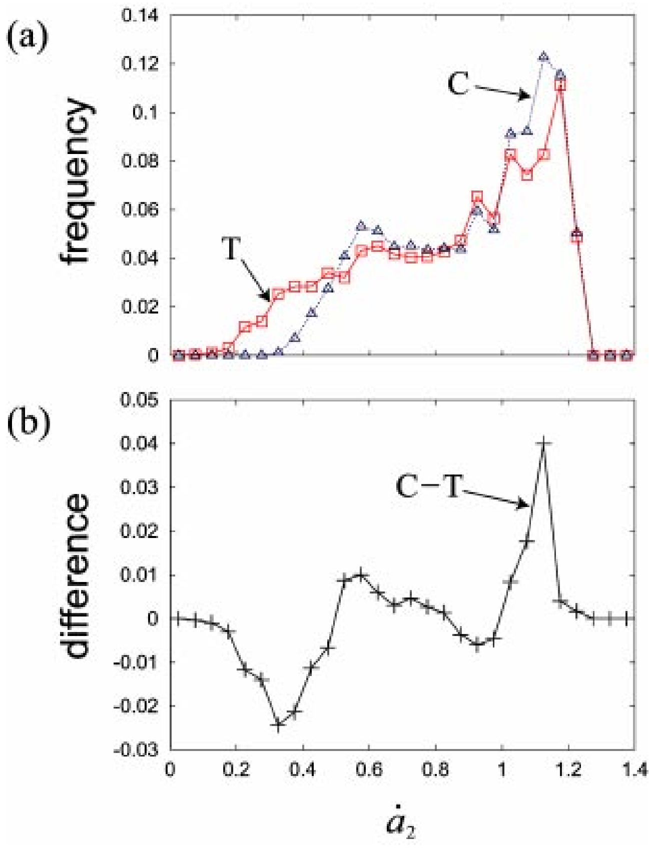

FIG. 13. Frequency distributions for $\dot{a}_2$ at the instant of crossing the line $a_2=0$ on gyration space (normalized to unity). Panel (a) shows the result for the dynamics under no gauge field (the constrained dynamics to the Eckart subspace) denoted as C (plotted with triangle) and that for the true dynamics under the influence of gauge field denoted as T (square). Panel (b) displays the difference $C-T$, which certainly shows a clear shift from the low to high values in $\dot{a}_2$. Total internal energy of the trajectories is $E=-1.20\varepsilon$.

remarkable fact is that the collinear saddle region of the M_3 cluster is dynamically stabilized due to the DCF. We have shown that an effective potential, which is a sum of a potential function and the potential arising from the DCF, holds a new "basin" around the collinear transition state. Owing to this basin structure, the M_3 cluster can be trapped in the transition region for a long time and recrosses the dividing surface many times. The present approach has provided a unified view of the recrossing problem and regularity of reactive trajectories in the saddle region.

It would be worthwhile to mention here that the above results have been observed in the four atom cluster M_4.[39] In the tetraatomic clusters in three-dimensional space, internal space is parametrized by three gyration radii (a_1,a_2,a_3) and three hyperangles $(\varphi_1,\varphi_2,\varphi_3)$. During collective isomerizing motions, through which one tetrahedral isomer turns to the other permutationally distinct tetrahedron via a planar rhombus shaped transition state, the three hyperangles are "locked" and two of the three gyration radii dominate the reaction. Therefore the reaction path for the M_4 cluster is essentially described with two gyration variables a_1 (the largest one) and a_3 (the smallest). The DCF also arises on three-dimensional gyration space in response to the variation of hyperangles, which distorts the M_4 cluster so as to enlarge the largest gyration radius a_1 and to diminish the absolute value of the smallest gyration radius a_3 along each principal axis. The transition state of planer rhombus structure is likewise stabilized and a trapped motion has been observed.

We have investigated kinematic effects associated with the Eckart frame, which is the most standard body frame in the theories of molecular vibrations. We have found that the gauge field associated with the Eckart frame arising in the internal space, the roles of which do not seem to have been fully scrutinized in the conventional reaction-rate theories, has an effect of inhibiting the isomerization reaction of the M_3 cluster significantly. Our numerical results suggest that the reaction rate theories that disregard the effects of the gauge field could *overestimate* the reaction rates up to about 20–30%. We have also presented a theoretical mechanism of this numerical fact, which highlighted the above stated roles of the DCF again.

It is obvious that the gauge field in the internal dynamics should have an important effect in a statistical theory of chemical reaction. First, the volume of the corresponding phase space, both in the reactant and transition state, is significantly changed. In fact, a very naive treatment of the reaction rate by an expression "the number of states at the transition state divided by the density of states at the equilibrium structure" gives rise to the similar estimate of the difference between the true dynamics and the dynamics under no gauge field. Second, the effective potential of Fig. 9, the basin structure of which accounts for the recrossing dynamics in a unified manner, can be vital to a reconsideration of the underlying statistical hypothesis. All these materials will be fully discussed in our future publications.

Finally we would like to note that our preliminary study on large molecules shows that the effects of the gauge field associated with the Eckart frame and the resultant effects of the non-Euclidean nature of internal space are never small. It is not correct to expect that such effects may become relatively negligible as a molecule becomes large. Our analysis presented above and preliminary studies as well thus suggest that the essential roles of the intrinsic metric in internal space together with those of the gauge field should be further revealed particularly in polyatomic molecules with many degrees of freedom.

ACKNOWLEDGMENTS

This work has been supported in part by the Grant-in-Aid for the 21st Century COE Program for Frontiers in Fundamental Chemistry from the Ministry of Education, Culture, Sports, Science and Technology of Japan. One of the authors (T.Y.) has been supported by Research Fellowships of the Japan Society for the Promotion of Science for Young Scientists.

[1] R. S. Berry, T. L. Beck, H. L. Davis, and J. Jellinek, Adv. Chem. Phys. **70**, 75 (1988); J. Jellinek, T. L. Beck, and R. S. Berry, J. Chem. Phys. **84**, 2783 (1986); F. G. Amar and R. S. Berry, *ibid.* **85**, 5943 (1986).
[2] P. Labastie and R. L. Whetten, Phys. Rev. Lett. **65**, 1567 (1990).
[3] C. Seko and K. Takatsuka, J. Chem. Phys. **104**, 8613 (1996); **108**, 4924 (1998); **109**, 4768 (1998); K. Takatsuka and C. Seko, *ibid.* **105**, 10356 (1996); **110**, 3263 (1999); T. Yanao and K. Takatsuka, Chem. Phys. Lett.

313, 633 (1999); K. Takatsuka and T. Yanao, J. Chem. Phys. **113**, 2552 (2000).

[4] C. Amitrano and R. S. Berry, Phys. Rev. Lett. **68**, 729 (1992); Phys. Rev. E **47**, 3158 (1993); R. J. Hinde, R. S. Berry, and D. J. Wales, J. Chem. Phys. **96**, 1376 (1992).

[5] R. J. Hinde and R. S. Berry, J. Chem. Phys. **99**, 2942 (1993).

[6] T. Komatsuzaki and M. Nagaoka, J. Chem. Phys. **105**, 10838 (1996); T. Komatsuzaki and R. S. Berry, J. Chem. Phys. **110**, 9160 (1999); **115**, 4105 (2001).

[7] J. I. Steinfeld, J. S. Francisco, and W. L. Hase, *Chemical Kinetics and Dynamics* (Prentice-Hall, Englewood Cliffs, NJ, 1989).

[8] W. H. Miller, J. Phys. Chem. A **102**, 793 (1998); Faraday Discuss. **110**, 1 (1998).

[9] R. S. Berry, Chem. Rev. **93**, 2379 (1993); P. A. Braier, R. S. Berry, and D. J. Wales, J. Chem. Phys. **93**, 8745 (1990); M. A. Miller, J. P. K. Doye, and D. J. Wales, *ibid.* **110**, 328 (1999).

[10] F. H. Stillinger and T. A. Weber, Phys. Rev. A **25**, 978 (1982); R. A. LaViolette and F. H. Stillinger, J. Chem. Phys. **83**, 4079 (1985).

[11] J. N. Onuchic, Z. A. Luthey-Schulten, and P. G. Wolynes, Annu. Rev. Phys. Chem. **48**, 545 (1997).

[12] K. A. Dill and H. S. Chan, Nat. Struct. Biol. **4**, 10 (1997); C. M. Dobson, A. Šali, and M. Karplus, Angew. Chem., Int. Ed. Engl. **37**, 868 (1998).

[13] R. Montgomery, in *The Geometry of Hamiltonian Systems*, edited by T. Ratiu (Springer-Verlag, 1991), p. 403.

[14] R. Montgomery, Nonlinearity **9**, 1341 (1996).

[15] A. Shapere and F. Wilczek, Phys. Rev. Lett. **58**, 2051 (1987); J. Fluid Mech. **198**, 557 (1989).

[16] C. Eckart, Phys. Rev. **47**, 552 (1935).

[17] E. B. Wilson, J. C. Decius, and P. C. Cross, *Molecular Vibrations* (McGraw-Hill, New York, 1955).

[18] J. D. Louck and H. W. Galbraith, Rev. Mod. Phys. **48**, 69 (1976).

[19] B. T. Sutcliffe, in *Quantum Dynamics of Molecules*, edited by R. G. Wooley (Plenum, New York, 1980), p. 1.

[20] W. H. Miller, N. C. Handy, and J. E. Adams, J. Chem. Phys. **72**, 99 (1980).

[21] M. Page and J. W. McIver, Jr., J. Chem. Phys. **88**, 922 (1988).

[22] A. Guichardet, Ann. I.H.P. Phys. Theor. **40**, 329 (1984).

[23] A. Tachibana and T. Iwai, Phys. Rev. A **33**, 2262 (1986).

[24] T. Iwai, Ann. I.H.P. Phys. Theor. **47**, 199 (1987); T. Iwai, J. Math. Phys. **28**, 964 (1987); **28**, 1315 (1987); T. Iwai, Phys. Lett. A **162**, 289 (1992).

[25] R. G. Littlejohn and M. Reinsch, Rev. Mod. Phys. **69**, 213 (1997).

[26] W. Zickendraht, J. Math. Phys. **10**, 30 (1969).

[27] X. Chapuisat and A. Nauts, Phys. Rev. A **44**, 1328 (1991).

[28] X. Chapuisat, Phys. Rev. A **45**, 4277 (1992).

[29] X. Chapuisat, J. P. Brunet, and A. Nauts, Chem. Phys. Lett. **136**, 153 (1987).

[30] A. Kuppermann, J. Phys. Chem. **100**, 2621 (1996); J. Phys. Chem. A **101**, 6368 (1997).

[31] F. T. Smith, Phys. Rev. **120**, 1058 (1960).

[32] R. G. Littlejohn and M. Reinsch, Phys. Rev. A **52**, 2035 (1995).

[33] R. G. Littlejohn, K. A. Mitchell, V. A. Aquilanti, and S. Cavalli, Phys. Rev. A **58**, 3705 (1998).

[34] R. G. Littlejohn, K. A. Mitchell, M. Reinsch, V. Aquilanti, and S. Cavalli, Phys. Rev. A **58**, 3718 (1998).

[35] V. Aquilanti and S. Cavalli, J. Chem. Phys. **85**, 1355 (1986).

[36] G. Strang, *Linear Algebra and its Applications* (Academic, New York, 1976).

[37] J. Costley and P. Pechukas, J. Chem. Phys. **77**, 4957 (1982).

[38] J. Manz, E. Pollak, and J. Römelt, Chem. Phys. Lett. **86**, 26 (1982).

[39] T. Yanao and K. Takatsuka, Phys. Rev. A **68**, 032714 (2003).